El Cezeri
Journal of Science and Engineering
ISSN: 2148-3736

Research Article

A Comparative Analysis of Elastic, Mechanical, and Thermoelectric Properties in Mg_2X (X =Si, Ge and Sn) Semiconducting Nanomaterials

Adwitiya Yadav[1a], Prashant Srivastav[1b], Pramod Kumar Yadawa[1c]
[1]Department of Physics, Prof. Rajendra Singh (Rajju Bhaiya) Institute of Physical Sciences for Study and Research, V. B. S. Purvanchal University, Jaunpur, India

adwitiya94@gmail.com

DOI: 10.31202/ecjse.1695273
Received: 08.05.2025 Accepted: 19.09.2025
How to cite this article:
Adwitiya Yadav, Prashant Srivastav, Pramod Kumar Yadawa, "A Comparative Analysis of Elastic, Mechanical, and Thermoelectric Properties in Mg_2X (X =Si, Ge and Sn) Semiconducting Nanomaterials", El-Cezeri Journal of Science and Engineering, Vol: 12, Iss: 3, (2025), pp.(283-297).
ORCID: [a]0009-0009-0978-6111, [b]0000-0003-4596-6258, [c]0000-0002-9525-2205.

ABSTRACT: The elastic, mechanical, thermodynamic, and ultrasonic properties of Mg_2X (X = Si, Ge, Sn) composite semiconducting nanomaterials were systematically investigated using Lennard-Jones potential analysis. This approach enabled the evaluation of second- and third-order elastic coefficients. Our findings, corroborated through comparative analysis with existing literature, reveal that higher-order elastic constants exhibit a slight initial increase, while subsequent values show minimal variation from Mg_2Si to Mg_2Sn. The elastic constants were further employed to assess the mechanical behavior of hexagonal Mg_2X nanomaterials via key parameters including Poisson's ratio, Young's modulus, bulk modulus, and related thermodynamic properties. Notably, the bulk modulus displays a consistent increase across the compositions. Despite the similar nanomaterial compositions, the calculated G/B ratio, an indicator of ductility versus brittleness, was found to be ~0.976, suggesting predominantly ionic bonding in Mg_2X compounds. Thermal conductivity (k_min) was computed across the series, demonstrating a steady increase from Mg_2Si to Mg_2Sn, accompanied by a consistent hardness profile. Additionally, ultrasonic attenuation and velocity measurements were conducted, revealing composition-dependent variations. The materials exhibit minimum attenuation at initial states, indicating maximum purity, while the lowest attenuation values correspond to enhanced ductility. Previous first-principles studies on Mg_2X (X = Si, Ge, Sn) have primarily focused on electronic and thermoelectric properties, with limited attention to elastic, mechanical, and ultrasonic behavior at the nanoscale. This study fills that gap by providing comprehensive insights into higher-order elastic constants and their impact on the mechanical and thermoelectric performance of Mg_2X nanomaterials.

Keywords: Elastic properties, Mg_2X (X=Si, Ge, and Sn) composition, Mechanical properties, Thermal properties, Ultrasonic properties.

I. INTRODUCTION

The composite semiconducting nanomaterials Mg_2X (X = Si, Ge, Sn) exhibit exceptional properties—such as low electrical resistivity, low thermal conductivity, and high Seebeck coefficients [1,2] which make them highly attractive for integration into both conventional and next-generation high-performance energy storage systems as battery electrode materials. As members of the thermoelectric Mg_2X nanocomposite family, these compounds offer a compelling combination of electrical and thermal characteristics suited for advanced energy applications [3–5].

In addition, Mg_2X compounds possess relatively low band gaps (0.3–0.6 eV), rendering them suitable for optoelectronic applications, including infrared detectors and optical fiber technologies [6]. Magnesium itself is also considered a promising material for hydrogen storage, owing to its high hydrogen uptake capacity (7.6 wt.%). More recently, the Mg_2X system, where X belongs to group IV(B) of the periodic table (i.e., Si, Ge, Sn), has received growing attention in the search for novel intermetallic alloys with enhanced thermodynamic behavior for hydrogen storage, particularly at cryogenic temperatures [7].

The Mg_2X (X = Si, Ge, Sn) compounds are known to crystallize in three primary structures: hP6 (hexagonal), cF12 (cubic), and cF24 (cubic). Among these, recent studies have predominantly focused on the cubic cF12 phase due to its favorable structural and physical properties. Whitten et al. [8] and Chung et al. [9] employed a resonance method as early as 1965 to determine the elastic constants of cF12-Mg_2X in the temperature range of 80–300 K. Using these experimentally derived elastic constants along with optical data, they further computed the lattice vibrational frequencies.

Building on this foundational work, Murtaza et al. [10,11] investigated the thermoelectric, optoelectronic, and elastic properties of cF12-Mg_2X. Their findings revealed that as the composition varies, the bulk modulus increases while the lattice constant decreases—trends that contribute to the materials' narrow bandgaps and high thermal potential, making them highly suitable for optoelectronic and thermoelectric device applications. Furthermore, generalized gradient approximation (GGA) calculations of the thermodynamic and elastic parameters indicated that Mg_2Si exhibits superior structural stability, while cF12-Mg_2Ge demonstrates the strongest alloying capability among the three compositions [12].

Additionally, in cF12-Mg_2X (X = Si, Ge, Sn) compounds, the temperature dependence of the stiffness elastic coefficients Cij(T)C_{ij}(T)Cij(T) has been determined by correlating the equilibrium volume as a function of temperature V(T)V(T)V(T) with the stiffness coefficients Cij(V)C_{ij}(V)Cij(V), which are derived from volume-dependent phonon calculations [13]. First-principles studies on binary magnesium compounds have shown that Mg_2Si exhibits a mixed bonding character, incorporating both ionic and covalent components [14]. Specifically, the bonding in cF12-Mg_2Si is characterized by a complex interplay of metallic, ionic, and covalent interactions. This hybrid bonding nature contributes to the compound's structural stability and intrinsic brittleness, as revealed through detailed thermodynamic, elastic, and electronic structure analyses [15].

The pyroelectric, optoelectronic, and elastic properties of cF12-Mg_2X (X = Si, Ge, Sn, and Pb) reveal that while Mg_2Sn exhibits significant elastic anisotropy, both cF12-Mg_2Si and cF12-Mg_2Ge behave as nearly isotropic materials [16]. One of the key advantages of thermoelectric solid-state power generators lies in their simple architecture, absence of moving parts, and modest efficiency in converting thermal energy directly into electrical power [17]. As early as 1961, Nikitin et al. [18] recognized that Mg_2BIV compounds (BIV = Si, Ge, Sn) possessed a favorable combination of chemical and physical properties, making them promising candidates for the development of efficient thermoelectric materials. Their structural and electronic similarities to elemental group IV semiconductors further support their potential in thermoelectric applications [19, 20].

Among these, magnesium silicide (Mg_2Si), which crystallizes in the antifluorite structure, has been identified as a particularly promising material for thermoelectric energy conversion in the temperature range of 500–800 K. It is a narrow bandgap semiconductor with an indirect bandgap of approximately 0.77 eV [21, 22]. Moreover, Mg_2Si is abundant in the Earth's crust, non-toxic, and environmentally benign—distinct advantages over conventional thermoelectric materials such as PbTe and $CoSb_3$, which may pose environmental or health risks [23].

The anti-fluorite crystal structure (space group $Fm\bar{3}m$) of semiconducting magnesium silicide (Mg_2Si) and magnesium germanide (Mg_2Ge) has positioned these materials as strong candidates for high-performance thermoelectric applications. Their remarkable properties—including low electrical resistivity, low thermal conductivity, and high Seebeck coefficients—make them particularly attractive for energy conversion technologies [24]. Mg_2Si and Mg_2Ge exhibit a broad spectrum of temperature-dependent physical behaviors, largely governed by their lattice dynamical properties, making the understanding of their vibrational characteristics essential for optimizing performance.

Among the Mg_2X compounds (X = Si, Ge, Sn), Mg_2Si stands out as the only stoichiometric silicide with stable existence, distinguishing it from most other silicides. These materials have attracted significant attention in recent years due to their high thermoelectric efficiency, especially in the mid-temperature range of 500–800 K. Their suitability arises from a combination of high electrical conductivity and relatively high melting points—1358 K for Mg_2Si, 1030 K for Mg_2Sn, and 1390 K for Mg_2Ge—which enhance their thermal and mechanical robustness in demanding applications. Furthermore, Mg_2X compounds are lightweight materials exhibiting high specific strength, along with excellent elastic and mechanical properties, particularly in their nanocomposite semiconducting forms [25].

In this study, we investigate the single-crystal elastic constants—specifically the second-order (SOEC) and third-order (TOEC) elastic constants—along with key thermo-physical, ultrasonic, and thermal properties of Mg_2X (X = Si, Ge, and Sn) using Lennard-Jones potential analysis. The evaluated parameters include Debye velocity, Debye temperature, ultrasonic attenuation coefficient, stiffness constants, thermal relaxation time, Young's modulus (Y), Poisson's ratio, bulk modulus (B), shear modulus (G), and Pugh's ratio (B/G). This study aims to deliver a comprehensive understanding of the elastic and mechanical properties of Mg_2X nanomaterials, offering valuable insights for their application in next-generation energy storage and thermoelectric devices. These comprehensive insights provide valuable guidance for the future design and development of Mg_2X-based compositions for advanced functional and thermoelectric applications.

2. COMPUTATIONAL THEORY

2.1. Second order elastic constant & third-order elastic constant of Mg_2X (X=Si, Ge, and Sn)

To provide a concise description of the material's physical and mechanical properties as well as its anisotropic attenuation behavior, several theoretical approaches are available in addition to experimental methods that can be used to examine the previously mentioned characteristics through formulation. Among the researchers, the well-known Lennard-Jones interaction potential techniques are widely employed because of their high level of accuracy in producing results according to experimental standards. This evaluation provides definitions for the additional-order elastic constants, including the experimental material referred to as second-order (SOEC) and its third-order (TOEC) value, and this potential model's evaluation technique

demonstrates how the second-order elastic constants connected to materials with a hexagonal structure are influenced by the lattice parameters.

$$C_{IJ} = \frac{\partial^2 U}{\partial e_I \partial e_J}; \qquad \text{I or J} = 1\ldots6 \tag{1}$$

$$C_{IJK} = \frac{\partial^3 U}{\partial e_I \partial e_J \partial e_K}; \text{ I or J or K} = 1\ldots6 \tag{2}$$

Also the general potantial farmulation for the Lennard-Jones model is well defined by

$$\varphi(r) = -\frac{a_0}{r^m} + \frac{b_0}{r^n} \tag{3}$$

Where,$a_0 = 4\varepsilon\sigma^m$, and $b_0 = 4\varepsilon\sigma^n$ here m and n are fitting parameters and ε and σ are the inter-atomic potential parameters.

Equations 4 and 5 represent general mathematical simplifications, where the third-order elastic constants (TOECs) are decomposed into ten fundamental parametric forms, and the second-order elastic constants (SOECs) into six. This decomposition facilitates further simplification processes, enabling precise theoretical evaluation of the material properties previously described. These formulations for SOECs and TOECs are detailed in Equations 4 and 5, respectively [26].

$$\left.\begin{aligned} C_{11} &= 24.1\ \mathrm{p}^4 C' \\ C_{12} &= 5.918\ \mathrm{p}^4 C' \\ C_{13} &= 1.925\ \mathrm{p}^6 C' \\ C_{33} &= 3.464\ \mathrm{p}^8 C' \\ C_{44} &= 2.309 p^4 C' \\ C_{66} &= 9.851\ \mathrm{p}^4 C' \end{aligned}\right\} \tag{4}$$

$$\left.\begin{aligned} C_{111} &= 126.9p^2B + 8.853p^4C' \\ C_{112} &= 19.168p^2B - 1.61p^4C' \\ C_{113} &= 1.924p^4B + 1.155p^6C' \\ C_{123} &= 1.617p^4B - 1.155p^6C' \\ C_{133} &= 3.695p^6B \\ C_{155} &= 1.539p^4B \\ C_{144} &= 2.309p^4B \\ C_{344} &= 3.464p^6B \\ C_{222} &= 101.039p^2B + 9.007p^4 \\ C_{333} &= 5.196p^8B \end{aligned}\right\} \tag{5}$$

Here, where p = c/a, is an axial ratio for the hexagonal material or compound and

$$C' = \chi\, \mathrm{a} / \mathrm{p}^5, \qquad B\psi\, \mathrm{a}^3 = /p^3,$$
$$\chi = (1/8)[\{n - m)\}/\{\mathrm{a}^{n+4}\}], \qquad \psi = -\chi\, /\{6\, \mathrm{a}^2(m + b_0\, (nn + 6)\}$$

Is evaluated using integer values, and the Lennard-Jones potential variable, b_0, is widely known. Additionally, these characteristics may be changed even with a small change in temperature or attenuation because they are incredibly dependent on these factors.

2.2. Ultrasonic Velocity

In order to understand the crystallographic behavior of experimental substances, we have calculated the shear velocity (V_{S2}), quasishear velocity (V_{S1}), and atomic vibratory pattern contingent Ultrasonic longitudinal velocity (V_L) at different propagation inclinations along the unique axis (c-axis). Additionally, we have computed the Debye average velocity (V_D) and Debye temperature (θ_D) using the SOECs and TOECs, the elastic properties of nanomaterials have been a subject of extensive research. For instance, the measurement of elastic properties in epoxy resin/polyvinyl alcohol nanocomposites using ultrasonic wave velocities I. oral et al. [27], provides valuable insights into the methodology and applications of elastic property measurement, which are relevant to our study. Mathematics is used to figure out the direction and propagational angle-dependent ultrasonic shear and longitudinal wave velocity (V_L and V_S) for waves traveling alongside a z-axis in a crystal with a hexagonal shape.

$$\left.\begin{aligned} V_L^2 &= \{C_{33}\cos^2\theta + C_{11}\sin^2\theta + C_{44} \\ &\quad +\{[C_{11}\sin^2\theta - C_{33}\cos^2\theta \\ &\quad +C_{44}(\cos^2\theta - \sin^2\theta)]^2 \\ &\quad +4\cos^2\theta\sin^2\theta\,(C_{13}+C_{44})^2\}^{1/2}\}/2\rho \\ V_{S1}^2 &= \{C_{33}\cos^2\theta + C_{11}\sin^2\theta \\ &\quad +C_{44} - \{[C_{11}\sin^2\theta - C_{33}\cos^2\theta \\ &\quad +C_{44}(\cos^2\theta - \sin^2\theta)]^2 \\ &\quad +4\cos^2\theta\sin^2\theta\,(C_{13}+C_{44})^2\}^{1/2}\}/2\rho \\ V_{S2}^2 &= \{C_{44}\cos^2\theta + C_{66}\sin^2\theta\}/\rho \end{aligned}\right\} \quad (6)$$

Also from the previously defined value of elastic constants along various tensor directions, we can also define the value of sound velocity in longitudinal and shear direction as [28].

$$V_L = \sqrt{\frac{C_{33}}{\rho}} \quad (7)$$

$$V_S = \sqrt{\frac{C_{44}}{\rho}} \quad (8)$$

where V_{S1}, V_{S2}, and V_L stand for longitudinal, quasi, and shear wave ultrasonic velocities, respectively. where the variables (V) stand for the material's density and the angle with the crystal's unique axis, respectively. Also, V_l : Longitudinal wave velocity, associated with compressional waves. V_s : Shear wave velocity, associated with transverse waves. V_D: Debye average velocity, derived from V_l and V_s, and related to the phonon transport and thermal properties of the material.

An essential physical measure for material characterization is the Debye Temperature (T_D), which is closely linked to the Debye Average Velocity (V_D). The formula can be used to determine the density of a material with a hexagonal structure.

$$d = \frac{2\mathrm{Mn}}{3\sqrt{3a^2cN_A}} \quad (9)$$

M, NA, and n stand for molecular weight, Avogadro number, and atoms per unit cell, respectively. At the low temperature in physics, the associated Debye average velocity is a crucial metric since ultrasonic velocities are dependent on elastic constants. It can be described in general as

$$V_D = \left[\frac{1}{3}\left(\frac{1}{V_L^3} + \frac{1}{V_{s1}^3} + \frac{1}{V_{s2}^3}\right)\right]^{-1/3} \quad (10)$$

Further, the Deby velocity relative Debye temperature for our experimental hexagonal material can be generally described by

$$T_D = \hbar V_D \frac{6\pi^2 n_a)^{\frac{1}{3}}}{K_B} \quad (11)$$

Where K_B: Boltzmann constant, n_a: atomic concentration; constant

Due to the advanced engineering application of experimental HCP material in a temperature and composition limit, it becomes important to investigate their thermophysical behavior at those extreme conditions. Utilizing the Debye model of heat capacity, we have calculated the thermal energy densities (E_0) and heat capacity (C_V) [29].

Within the scope of these experiments, the period of time taken during thermodynamic phonons to reassemble themselves following the propagation of an ultrasonic wave is known to be the corresponding thermal relaxation time (τ). It has a direct relationship with specific heat (C_V), Debye average velocity, and thermal conductivity (k) [30].

$$\tau = \tau_S = \tau_L/2 = \frac{3k}{C_V V_D^2} \quad (12)$$

Based on the experimental analysis of the evaluated physical properties, the material's stability, crystal structure, thermal conductivity, mechanical strength, and hardness can be reliably inferred from the calculated second-order elastic constants (SOECs). Furthermore, the Voigt–Reuss–Hill (VRH) approximation [31] has been employed to investigate variations in key mechanical parameters, including Pugh's ratio (B/G), Young's modulus (Y), Poisson's ratio (σ), bulk modulus (B), and shear modulus (G). The standard relationships for these parameters within the VRH framework are expressed below in Equation (13):

$$M = C_{11} + C_{12} + 2C_{33} - 4C_{13}$$

$$C^2 = (C_{11} + C_{12})C_{33} - 4C_{13} + C^2{}_{13}$$

$$B_R = \frac{C^2}{M}$$

$$B_V = \frac{2(C_{11} + C_{12}) + 4C_{13} + C_{33}}{9}$$

$$G_V = \frac{M + 12(C_{44} + C_{66})}{30}$$

$$G_R = \frac{5C^2C_{44}C_{66}}{2[3B_VC_{44}C_{66} + C^2(C_{44} + C_{66})]}$$
$$Y = \frac{9GB}{G + 3B}$$
$$B = \frac{B_V + B_R}{2} \quad (13)$$
$$G = \frac{G_V + G_R}{2}$$
$$\sigma = \frac{3B\text{-}2G}{2(3B+G)}$$

The lattice thermal conductivity (κ) was evaluated by following the Morelli and Slack [32] approach, which is given as equation 14:

$$k = AMT_D{}^3\delta^3/\gamma^2Tn^{2/3} \quad (14)$$

Ma (in amu) is the average atomic mass, θ_D is the Debye temperature, T is the temperature, δ3 is the amount of volume for each atom, γ is the Grüneisen number, and A represents the proportional constant. n is the total number of atoms per unit cell. Here the Grüneisien number determines the numerical value for the constant 'A', which is stated as follows.

$$A = 2.43 \times 10^{-8}/(1 - \frac{0.514}{\gamma} + \frac{0.228}{\gamma^2}) \quad (15)$$

γ is the Grüneisen number, which can be determined by $\gamma = \alpha B/(CV\acute{\rho})$,where α is the thermal volume expansion coefficient, B is bulk modulus, C_V is the heat capacity, and ρ is density of the material.

The relative values of the melting temperatures (T_m) of hexagonal crystals [33] Is also dependent on the value of certain elastic constants C_{11} and C_{33} which are defined as, melting temperatures (T_m)

$$T_m = 354 + \frac{4.5(2C_{11}+C_{33})}{3} \quad (16)$$

Where C_{11} and C_{33} are in GPa, and T_m is in K.

2.3. Attenuation

The ultrasonic attenuations in single crystal solids at high temperatures are mostly due to phonon-phonon interactions (Akhiezer loss) and thermoelastic relaxation mechanisms (thermoelastic loss). The formulation for estimating ultrasonic attenuation due to phonon-phonon interactions was developed by [34] and is given by:

$$(\alpha/f^2)_{Akh}=4\pi 2\tau E_0(D/3)/2\rho V^3 \quad (17)$$

The ultrasonic wave frequency is denoted by f, and the thermal energy density is denoted by E_0.
The thermoelastic loss $(\alpha / f^2)_{Th}$: equation as follows

$$(\alpha/f^2)_{Th} = 4\pi^2 < \gamma_i^j >^2 \frac{kT}{2\rho V_L^5} \quad (18)$$
$$\alpha_{long} = \frac{2\pi^2 f^2}{\rho V_l^3}\left(\frac{4}{3}\eta_e + \chi\right) \quad (19)$$
$$\alpha_{shear} = \frac{2\pi^2 f^2}{\rho V_S^3}\eta_e \quad (20)$$

The total consequence of ultrasonic attenuation $(\alpha/f^2)_{Total}$, caused by the thermoelastic loss and Akhieser losses exhibited in the longitudinal, shear mode of propagation, can be calculated as [35]:

$$(\alpha/f^2)_{Total} = (\alpha/f^2)_{Th} + (\alpha/f^2)_L + (\alpha/f^2)_S \quad (21)$$

Where$(\alpha/f^2)_{Th}$is the thermoelastic loss, while $(\alpha/f^2)_L$and $(\alpha/f^2)_S$ are the ultrasonic attenuation coefficients for the longitudinal wave and shear wave, correspondingly.

3. RESULTS AND DISCUSSION

3.1. Second order elastic constant & third-order elastic constant of Mg_2X (X=Si, Ge, and Sn)

In the present study on Mg_2X (X = Si, Ge, and Sn) composite semiconducting nanomaterials, we have successfully derived accurate values for various elastic coefficients—specifically six second-order elastic constants (SOECs) and ten third-order elastic constants (TOECs)—using an interaction potential approach. Based on our theoretical framework and comparative analysis, the obtained results show strong agreement with available experimental data, exhibiting minimal deviations and confirming the validity of our model.

Additionally, we have determined the essential lattice parameters for Mg_2X (X = Si, Ge, and Sn), where "a" represents the basal plane lattice constant and "p" denotes the axial ratio (p=c/a)(p = c/a)(p=c/a) for the hexagonal close-packed (HCP) structure [36]. The composition-dependent lattice constants for Mg_2Si, Mg_2Ge, and Mg_2Sn are found to be 4.629 Å, 4.739 Å, and 5.0913 Å, respectively, as illustrated in Figure 1. Corresponding densities of states (DOS) for each composition are also

provided. The constant value of Leonard Jones potential constant "b_0" is also evaluated with mathematical simulation manipulation technique and finally taken at $5.07\times e^{-62}$,$6.37\times e^{-62}$,$1.56\times e^{-66}$ erg cm^3, respectively, for different nanomaterials.

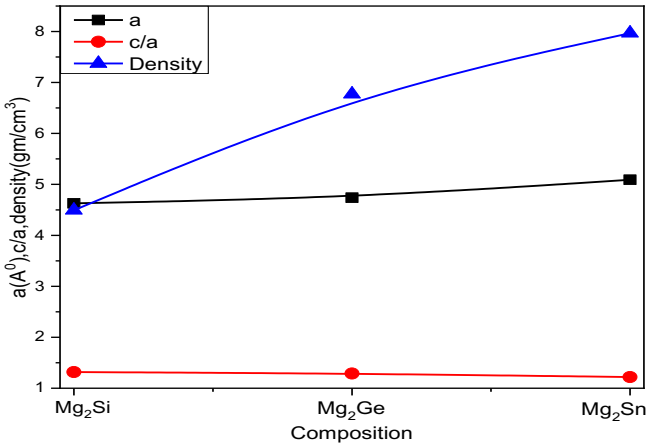

Figure 1. The dedicated value of Lattice constant a (Å), Bessel plane distance c/a, and relative density, with nanomaterial composition Mg_2X (X=Si, Ge, and Sn)

Additionally, on the basis of the above-mentioned and evaluated data, the evaluated values of the second and third-order elastic constants of the Mg_2X (X=Si, Ge, and Sn) are depicted in Figure 2 and Figure 3, respectively.

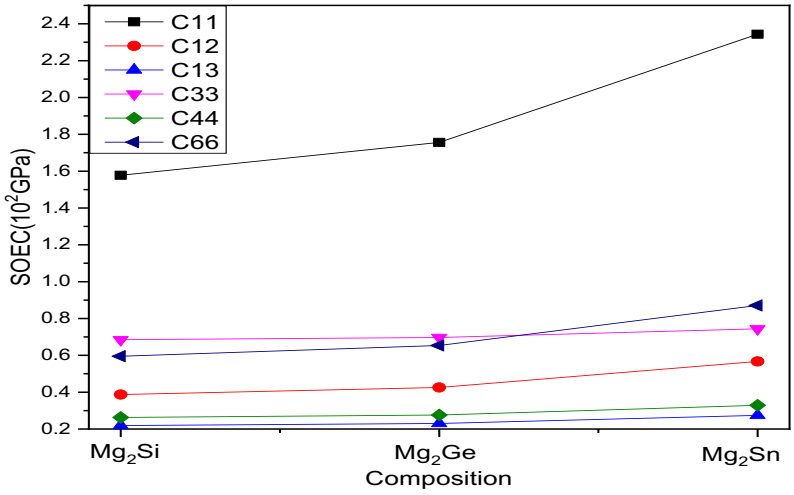

Figure 2. The variation in the respective values of SOECs with nanomaterial composition Mg_2X (X=Si, Ge, and Sn)

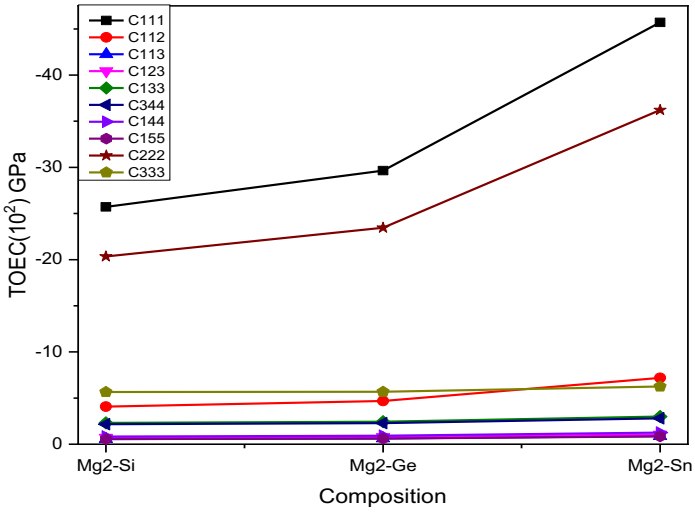

Figure 3. The variation in the respective values of TOECs with nanomaterial composition Mg_2X (X=Si, Ge, and Sn)

The above Figure 2 depicts the evaluated variation of SOEC of intrinsic semiconductor material (Si, Ge, and Sn) with the moderate band gap conducting material Mg in the composite format. On the basis of data analysis for the particular HCP complex material Mg_2X (X=Si, Ge, and Sn), we can conclude that the negative values of TOECs indicate the presence of strain within the material Mg in composition. This is aligned with previous investigations on materials with hexagonal structures, affirming the theoretical framework's accuracy in valuing higher-order elastic coefficients. As a result, the theory used to investigate higher-order elastic coefficients is justified using Eqs. 1 and 2. For HCP structure material stability, here the five different SOECs (C_{ij}, namely C_{11}, C_{12}, C_{13}, C_{33}, and C_{44}) satisfy Born-Huang's norms [37]. This Mg_2X (X=Si, Ge, and Sn) is mechanically stable because it is evident that the positive elastic constant values satisfy Born-mechanical Huang's stability constraints defined as.

$$\acute{C}_{44} > 0,\ \acute{C}_{11} - |\acute{C}_{12}| > 0$$

$$(\acute{C}_{11} + \acute{C}_{12})\,\acute{C}_{33} - 2\,\acute{C}^2_{13} > 0 \tag{22}$$

Where $\acute{C}_{jj} = \acute{C}_{jj} - P$, (P=1, 3, 5). $\acute{C}_{12} = C_{12} + P$, $\acute{C}_{13} = C_{13} + P$

3.2. Mechanical Property

As the composition varies from Si to Ge and Sn, the density of the Mg-based compounds increases, while their corresponding atomic volume decreases, as illustrated in Figure 4. The values of bulk modulus (B), Young's modulus (Y), and shear modulus (G) for Mg_2X (X = Si, Ge, and Sn) are observed to increase progressively with changes in composition. This trend reflects an enhancement in the stiffness and bonding strength of the nanomaterials.

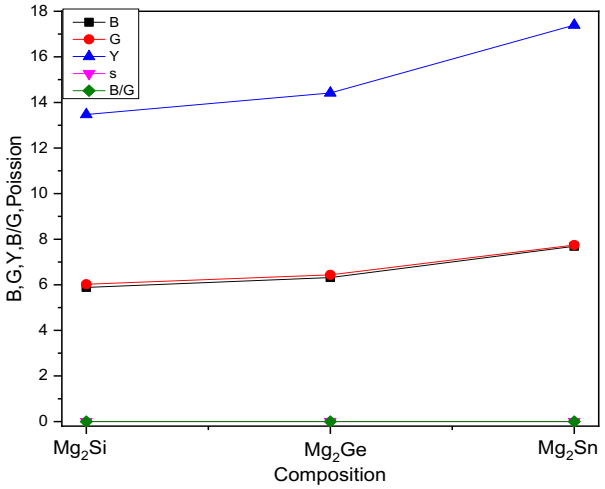

Figure 4. B, G, Y, B/G, σ with nanomaterial composition Mg_2X (X=Si, Ge, and Sn)

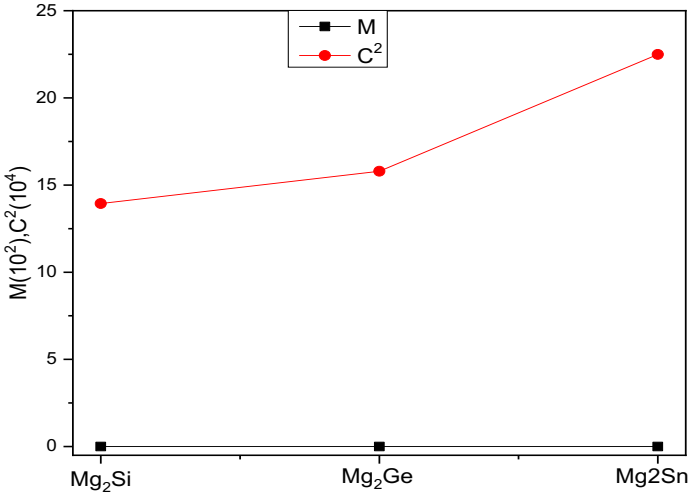

Figure 5. M, C^2 with nanomaterial composition Mg_2X (X=Si, Ge, and Sn)

Additionally, the G/B ratio, which is 0.97, 0.98, and 0.99 for Mg_2Si, Mg_2Ge, and Mg_2Sn respectively, signifies a predominant ionic bonding character within these compounds. This ratio, along with the B/G and Poisson's ratio (σ), provides valuable insights into the mechanical behavior of the materials, particularly in predicting their brittleness or ductility. Materials with $\sigma=0.23\leq0.26$ and $B/G=1.52\leq1.75$ are typically considered brittle, or else they are ductile in nature [38]. Our results for B/G indicate that the Mg_2X (X=Si, Ge, and Sn) is brittle in nature with nanomaterial composition because they are under their critical levels. The value of σ, which should perfectly be less than 0.5 for elastic and stable materials, is found to be within an acceptable range for composite. B/G ratio below 1.75 typically signifies brittleness, which is consistent with the behavior observed in Mg_2X compositions. In the below section, we have demonstrated the relative values of Voigt–Reus' constants (M and C^2), Br (x 10^{10} Nm^{-2}), Bv (x 10^{10} Nm^{-2}), Gr (x 10^{10} Nm^{-2}), Gv (x $10^{10}Nm^{-2}$), Y (x $10^{10}Nm^{-2}$) for Mg_2X (X=Si, Ge, and Sn).

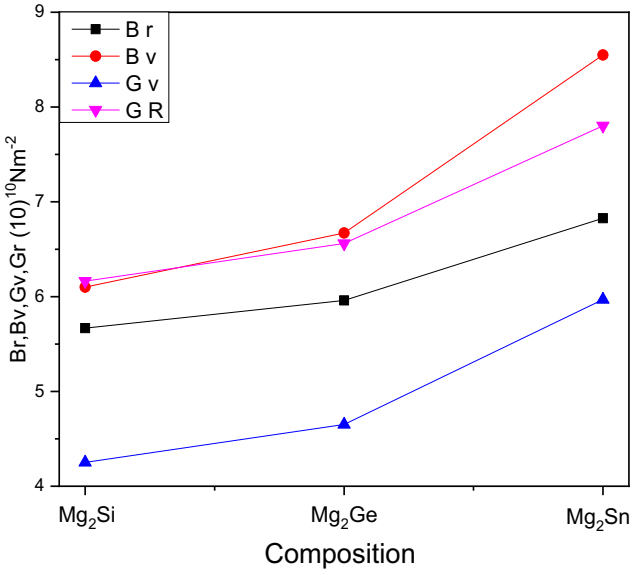

Figure 6. B_r, B_v, G_v, and G_r, with nanomaterial composition. Mg_2X (X=Si, Ge, and Sn)

In addition to the mechanical properties discussed above, the melting temperature serves as a critical parameter in the development of materials with enhanced thermal stability, ductility, and brittleness. The melting temperature (Tm) and hardness (Hv) of Mg_2X (X = Si, Ge, and Sn) have been systematically investigated and are presented in Figure 7, illustrating their variation as a function of composition.

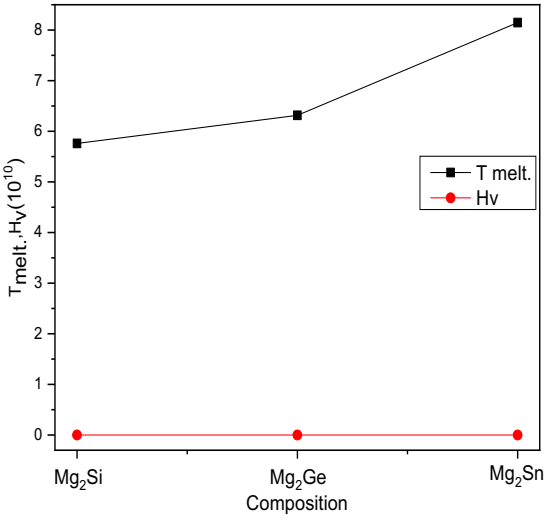

Figure 7. Hardness (H_v), melting temperature (T_m) with nanomaterial composition Mg_2X (X=Si, Ge, and Sn)

Table 1 demonstrates that elastic anisotropy can be effectively described by the unified anisotropic in elasticity may always be explained by the unified anisotropic index (A^U), percent anisotropic (AB and AG), and shear anisotropy factors (A_1, A_2, and A_3).

Table 1 shows that under different compositions of Mg_2X (X=Si, Ge, and Sn), AB has a higher percentage of anisotropy than AG. This suggests that the bulk modulus is less oriented than the shear modulus. A_1, A_2, and A_3 findings with nanomaterial are also displayed in Table 1. If $A_1 = A_2 = A_3 = 1$, the substance is an isotropic crystal. According to the findings, composition Mg_2X (X=Si, Ge, and Sn) is an anisotropic crystal absent in any other circumstances. With nanomaterial, the universal anisotropic index (A^U) deviates from zero, which is known as the highly single crystal anisotropy [39].

Table 1. Various anisotropy constants with their relative poisson's ratio for nanomaterial composition Mg_2X (X=Si, Ge, and Sn)

Composition	A^U	A_1	A_2	A_G	A_3	σ
Mg_2Si	**-1.47**	0.577	0.441	0.395	1.003	0.118
Mg_2Ge	**-1.33**	0.588	0.422	0.395	1.000	0.119
Mg_2Sn	**-0.92**	0.479	0.377	0.395	1.003	0.122

It is clear form Figure 8 that for all temperature, the values of D_S are larger than those of D_l for all composition nanomaterials. It indicates that for the shear ultrasonic wave the transformation of ultrasonic energy into thermal energy is less than for the longitudinal ultrasonic wave.

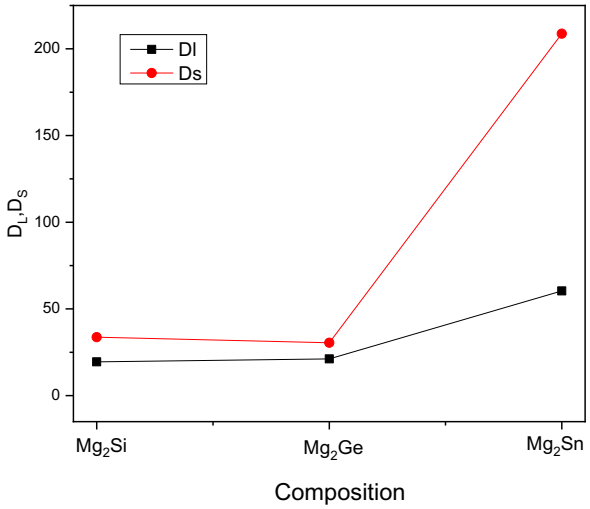

Figure 8. Variation of D_L, D_S with nanomaterial composition Mg_2X (X=Si, Ge, and Sn)

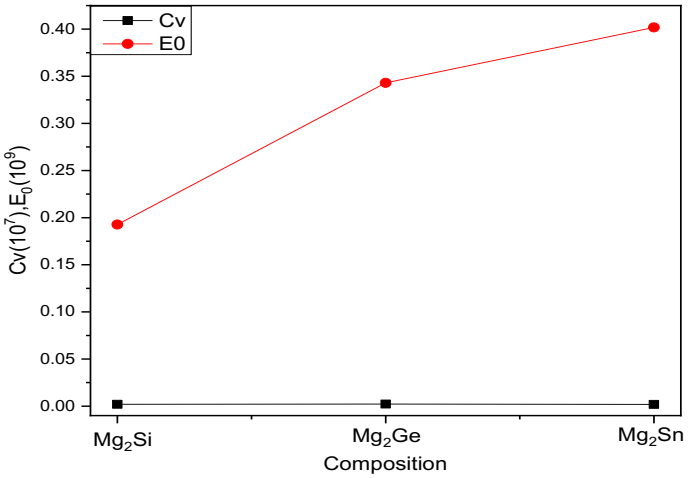

Figure 9. Variation of E_o and C_v with nanomaterial composition Mg_2X (X=Si, Ge, and Sn)

3.3. Ultrasonic velocity and allied parameters

The below Figures 10-13 demonstrate the angular dependency of ultrasonic velocities (V_L, V_{S1}, V_{S2}, V_D) with varying composition along the z-direction for the Mg_2X (X=Si, Ge, and Sn). In Figs. 10 and 11, the z-axis of the Mg_2X (X=Si, Ge, and Sn) correlates directly to the minima and maxima of the ultrasonic velocities V_L and V_{S1}. and the value of V_{S2} is demonstrated

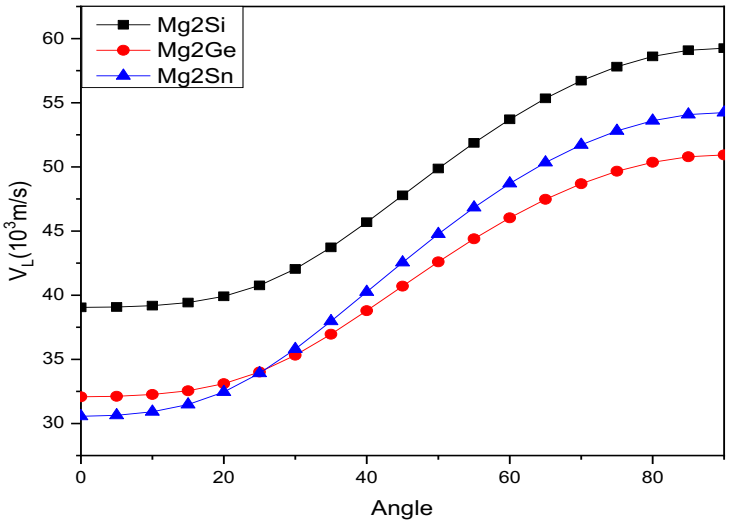

Figure 10. V_L vs. "Θ" for different nanomaterial compositions Mg_2X (X=Si, Ge, and Sn)

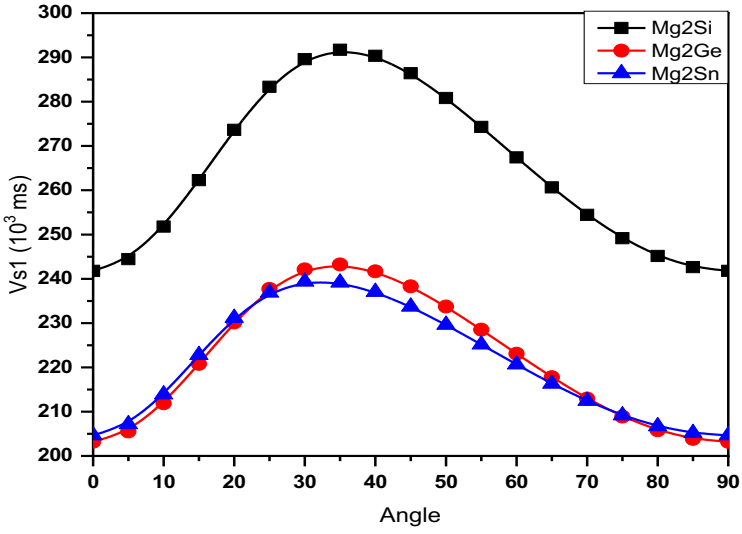

Figure 11. Vs_1 vs "Θ" for different nanomaterial compositions Mg_2X (X=Si, Ge, and Sn)

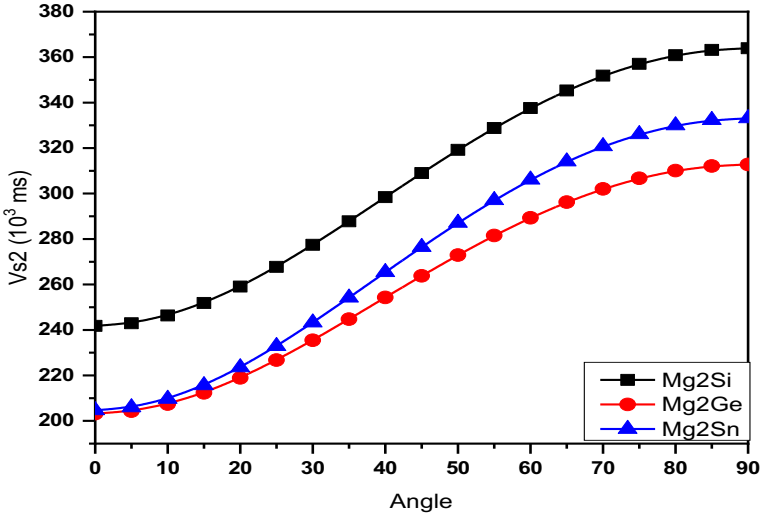

Figure 12. Vs_2 vs "Θ" for different nanomaterial compositions Mg_2X (X=Si, Ge, and Sn)

in Fig. 12, and it is clear from the see-through that its values rise with the angular spread along the z-direction. The combined effects of SOECs and ρ (density) are held responsible in Favor of the uncharacteristic behavior of angle-dependent velocity. This effort's discovery of the angle (Ɵ)-dependent velocity (V) curves is similar to those found for other hcp nanomaterials. This justifies the angle dependence of metal velocities [40]. Here, the V_D value rises with increasing angle and reaches its maximum at 55.0 degrees in figure 13. The relative value of the Debye average velocity is also influenced by the variation in the fundamental ultrasonic velocities, V_L, V_{S1}, and V_{S2}, which are used to evaluate V_D. Additionally, here When the z-axis of this crystal is at 55°, the average sound wave velocity shows a maximum.

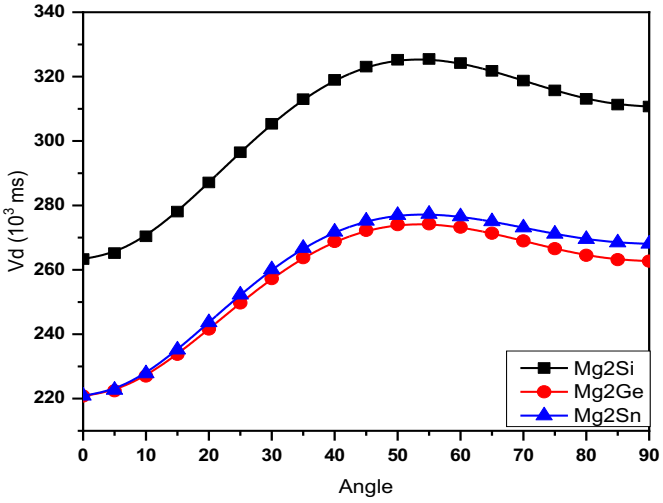

Figure 13. V_D vs "Ɵ" for different nanomaterial compositions Mg_2X (X=Si, Ge, and Sn)

In this section, Figure 14 presents a graphical depiction of the calculated thermal relaxation time, illustrating its variation with composition across different angular orientations. Here, the reciprocal characteristics of V_D, which are relative to $\tau \propto 3k/C_V V_D^2$ is evaluated, and here we can conclude that the value of thermal relaxation time for the Mg_2X (X=Si, Ge, and Sn) is highly dependent on the value of the Fermi radius and can be affected by 'k'. The hexagonal structure of the Mg_2X (X=Si, Ge, and Sn) is explained by the computation. The minimum value of the thermal relaxation time (τ\tauτ) occurs along the wave propagation direction at an angle of 55°, indicating the shortest re-establishment time for thermally generated phonons and their equilibrium distribution. Consequently, the presence of phonon–phonon (p–p) interactions and the associated thermal relaxation give rise to ultrasonic attenuation observed in the material along this direction.

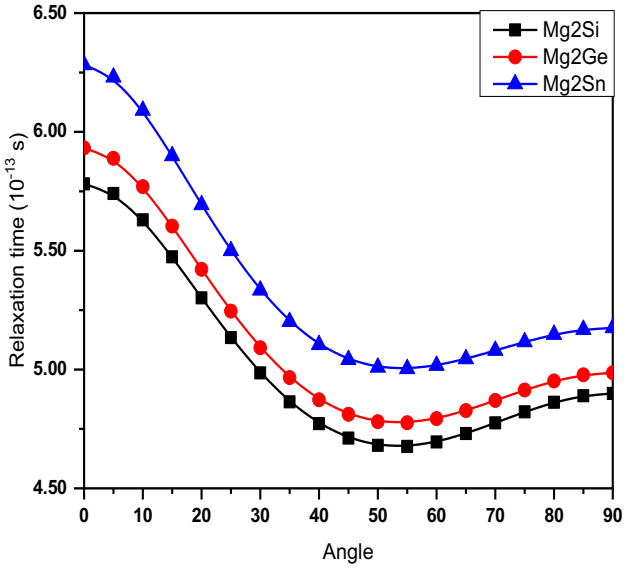

Figure 14. Relaxation time vs "Ɵ" with z- axis of crystal for different nanomaterial compositions Mg_2X (X=Si, Ge, and Sn)

3.4. Ultrasonic attenuation due to phonon-phonon interaction and thermal relaxation phenomena

In analyzing the ultrasonic attenuation, it is assumed that the wave flows along the z-axis of nanomaterial composition Mg_2X (X=Si, Ge, and Sn). The Attenuation coefficient is alienated over frequency squared for longitudinal wave $(\alpha/f^2)_L$ and for shear wave $(\alpha/f^2)_s$ under the condition $\omega\tau<<1$ at various compositions is calculated using Eq. 11. The thermo-elastic loss by frequency squared $(\alpha/f^2)_{th}$ is calculated using Eq. 11, and Table 2 illustrates the ultrasonic attenuation value resulting from the thermoelastic relaxation mechanism $(\alpha/f^2)_{th}$.

It is assumed that the wave propagates down the z-axis of the Mg_2X (X=Si, Ge, and Sn) compound when computing ultrasonic attenuation (UA). Eqn. 14,15, and 16 is used for calculating the attenuation coefficient divided by frequency squared (α/f^2) Akh for the wave's longitudinal direction (α/f^2) L and for the shear wave (α/f^2). Table 2 presented values of the composition-dependent longitudinal, shear and total attenuation of the Mg_2X (X=Si, Ge, and Sn**).** Energy losses $(\alpha/f^2)_{Akh}$ are substantially proportional to D, E_0, and V^{-3} (Eq. 11). Thus, in the nanomaterial composition Mg_2X (X=Si, Ge, and Sn), E_0 and K have a significant impact on Akhieser losses. The thermo-elastic loss for the nanomaterial composition Mg_2X (X=Si, Ge, and Sn) is to be substantially less than the Akhieser loss, indicating that the p-p interaction mechanism-induced ultrasonic attenuation dominates over the thermoelastic loss. Total attenuation is mainly driven by two variables, namely thermal energy density and thermal conductivity. Thus, although nano material compositions of Mg_2X (X=Si, Ge, and Sn) are the least ductile, they show their purest form at for different nanomaterial compositions and show additional ductility, as shown by the minimal attenuation. Hence, the nanomaterial composition Mg_2X (X=Si, Ge, and Sn) will have the lowest impurity content at ambient compositions.

Table 2. Long. & Shear attenuation for different nanomaterial composition Mg_2X (X=Si, Ge, and Sn)

Composition	$\left\{\frac{\alpha}{f^2}\right\}_{shear}$ (10^{-18}) Nps^2m^{-1}	$\left\{\frac{\alpha}{f^2}\right\}_{Th}$ $(10^{-21})Nps^2m^{-1}$	$\left\{\frac{\alpha}{f^2}\right\}_{long}$ (10^{-18}) Nps^2m^{-1}	$\left\{\frac{\alpha}{f^2}\right\}_{Total}$ (10^{-18}) Nps^2m^{-1}
Mg_2Si	3.155	9.598	2.130	5.295
Mg_2Ge	14.361	14.061	5.071	19.440
Mg_2Sn	101.430	23.521	17.634	119.086

In the present study, it is observed that ultrasonic waves predominantly propagate along the z-axis of the Mg_2X (X = Si, Ge, and Sn) compositions. Equations.17 clearly show that the Akh. Types of energy loses (α/f^2) Akh proportionate to D, E_0, τ, and V^{-3}. E_0' and V' are rising with composition Mg_2X (X=Si, Ge, and Sn), as seen in Figure 9. Therefore, in Mg_2X (X=Si, Ge, and Sn), Consequently, the Akhieser losses in Mg_2X nanomaterials are strongly influenced by the values of E_0 and the thermal conductivity k. A reduction in thermal conductivity leads to a notable increase in ultrasonic attenuation (UA). This suggests that UA is significantly governed by phonon–phonon (p–p) interaction mechanisms. However, due to the lack of sufficient experimental and theoretical data on ultrasonic attenuation in these specific materials, direct comparison and validation remain limited.

As shown in Table 2, the thermo-elastic loss in the nanomaterial composition Mg_2X (X = Si, Ge, and Sn) is significantly lower than the Akhieser loss. According to Equation (18), the primary contributor to total ultrasonic attenuation is Akhieser-type attenuation (UA), which is predominantly governed by phonon–phonon (p–p) interactions for both longitudinal and shear waves. The two key factors influencing total attenuation are thermal energy density and thermal conductivity.

The observed minimum attenuation values suggest that, although Mg_2X compositions are relatively less ductile, they exhibit characteristics of high purity. Additionally, ductility improves progressively across the compositions from Si to Sn. As a result, the compound with the lowest impurity level at room temperature is inferred to be Mg_2Si.

Furthermore, Mg_2Si demonstrates the highest ultrasonic velocities among the compositions, indicating superior ductility. Since attenuation $\alpha \propto V^3$, it is expected to reach its maximum in Mg_2Si. The minimal ultrasonic attenuation (UA) values for Mg_2Si further confirm the structural stability of its hexagonal phase.

4. CONCLUSIONS

Based on the comprehensive analysis of the Mg_2X (X = Si, Ge, and Sn) nanomaterial system, the following conclusions have been drawn:

- The standard computational approach used to determine higher-order elastic coefficients for hexagonal nanomaterials, based on the Lennard-Jones potential model, has proven effective and applicable to the Mg_2X (X = Si, Ge, and Sn) compositions.
- The evaluated elastic properties confirm that the Mg_2X nanomaterials are mechanically stable across all compositions.
- Young's modulus for these nanomaterials demonstrates greater anisotropy compared to the bulk modulus, as indicated by various anisotropy indices, suggesting direction-dependent mechanical behavior.

- The thermal relaxation time (τ) for all Mg_2X compositions is found to be on the order of 10^{-13} seconds, supporting their classification as intermetallic nanomaterials. Notably, the minimum value of τ along the wave propagation direction at 550 K implies the fastest phonon redistribution in this direction.
- The G/B ratios for Mg_2Si, Mg_2Ge, and Mg_2Sn were 0.97, 0.98, and 0.99, respectively, confirming their brittle nature.
- The dominant contribution of p–p interactions to ultrasonic attenuation (U.A.) plays a key role in influencing the thermal conductivity of these nanomaterials.
- Among all compositions, Mg_2Si exhibits superior mechanical properties, with stronger ionic bonding characteristics compared to Mg_2Ge and Mg_2Sn.
- The Mg_2X nanomaterials exhibit their highest purity at the initial Si-based composition and demonstrate enhanced ductility, as evidenced by the lowest ultrasonic attenuation values.

This research could help in computational as well as non-destructive classification of nanomaterials. These findings serve as the basis for further research into the major thermo-physical properties of other nanomaterials.

Acknowledgments

Authors are thankful to Center of Excellence grant from Department of Higher Education, Uttar Pradesh for financial support.

Authors' Contributions

Adwitiya Yadav: Conceptualization, Writing-original draft, Analyzing the results. Prashant Srivastav: Conceptualization, Writing-original draft, Editing, Analyzing the results. Pramod Kumar Yadawa: Review, Visualization, Supervision.

Competing Interests

The authors declare that there are no conflicts of interest related to this work. There are no known competing financial interests or personal relationships that could have influenced the findings presented in this study.

References

[1] V. K. Zaitsev, M.I. Fedorov, I. S. Eremin, and E. A. Gurieva, Thermoelectrics Handbook MacrotoNano, CRCPress, NewYork 2006.

[2] J. Tani, and H. Kido, "Impurity doping into Mg2Sn: A first-principles study," *PhysicaB Condensed Matter*, vol. 407**,** no. 17**,** pp. 3493-3498, 2012 https://doi.org/10.1016/j.physb.2012.05.008.

[3] M. R. Kavuncu, M. Ekrem, and N. Yazıcı, "Mechanical Properties and Damage Behavior of MWCNT Reinforced Polyurethane Nanocomposites", El-Cezeri Journal of Science and Engineering, vol. 9, no. 3, pp. 988–995, 2022, doi: 10.31202/ecjse.1018789.

[4] Y. Noda, H. Kon, Y. Furukawa, N. Otsuka, I. A. Nishida, and K. Masumoto, "Temperature dependence of thermoelectric properties of Mg2Si0.6Ge0.4*," Mater. Trans. JIM*, vol. 33, no. 9 pp. 851–855, 1992 https://doi.org/10.2320/matertrans1989.33.851

[5] F. Yu, J. X. Sun, and T. H. Chen, "High-pressure phase transitions of Mg2Ge and Mg2Sn: first-principles calculations," *PhysicaB,* vol 406**,** no. 9, pp. 1789–1794, 2011 https://doi.org/10.1016/j.physb.2011.02.029

[6] R. Janot, F. Cuevas, M. Latroche, and A. P. Guegan, "Influence of crystallinity on the structural and hydrogenation properties of Mg_2Xphases(X=Ni,Si,Ge,Sn)," *Intermetallics*, vol. 14, no. 2 pp. 163–169, 2006 https://doi.org/10.1016/j.intermet.2005.05.003

[7] J. Prigent, and M. Gupta, "Abinitio study of the hydrogenation properties of Mg-based binary and ternary compounds Mg2X(X=Ni,Si)and YMgNi4," *J.Alloy.Compd*., vol. 90**,** pp. 446–447, 2007 https://doi.org/10.1016/j.jallcom.2006.11.104

[8] W. B. Whitten, P. L. Chung, and G.C. Danielson, "Elastic constants and lattice vibration frequencies of Mg2Si," *J.Phys.Chem.Solids*, vol 26, no. 1 pp. 49–56, 1965 https://doi.org/10.1016/0022-3697(65)90071-5

[9] P. L. Chung, W. B. Whitten, G. C. Danielson, "Lattice dynamics of Mg2Ge", *J.Phys. Chem.Solids,* vol. 26, no. 12 pp.1753–1760, *1965* https://doi.org/10.1016/0022-3697(65)90206-4

[10] G. Murtaza, A. Sajidb, M. Rizwan, Y. Makagiwa, H. Khachai, M. Jibran, R. Khenata, and S. Bin Omran, "First principles study of Mg2X(X=Si,Ge,Sn,Pb): elastic, optoelectronic and thermoelectric properties", *Materials Science in Semiconductor Processing* , vol. 40, pp. 429–435, 2015 https://doi.org/10.1016/j.mssp.2015.06.075

[11] J. I. Tani, and H. Kido, "Lattice dynamics of Mg2Si and Mg2Ge compounds from first principles calculations," *Comp.Mater.Sci*, vol. 42, no. 3, pp. 531–536, 2008 https://doi.org/10.1016/j.commatsci.2007.08.018

[12] D. Zhou, J. Liu, S. Xu, and P. Peng, "Thermal stability and elastic properties of Mg2X(X =Si,Ge,Sn,Pb) phases from first-principle calculations", *Comp.Mater.Sci*, vol. 51, no. 1, pp. 409–414, 2012 https://doi.org/10.1016/j.commatsci.2011.07.012

[13] S. Ganeshan, S. L. Shang., Y. Wang, and Z. K. Liu, "Temperature dependent elastic coefficients of Mg2X (X=Si,Ge,Sn,Pb) compounds from first-principles calculations", *J. Alloy.Compd*, vol 498, no. 2, pp. 191–198, 2010 https://doi.org/10.1016/j.jallcom.2010.03.153

[14] S. Ganeshan, S. L. Shang, H. Zhang, Y. Wang, M. Mantina, and Z. K. Liu, "Elastic constants of binary Mg compounds from first-principles calculations", *Intermetallics*, vol. 17, no. 5 pp. 313–318, 2009 https://doi.org/10.1016/j.intermet.2008.11.005

[15] Z. W. Huang, Y. H, Zhao, H. Hou, and P. D, Han, "Electronic structural, elastic properties and thermodynamics of Mg17Al12, Mg2Si and Al2Y phases from first-principles calculations", *PhysicaB,* vol. 407, no. 7 pp. 1075–1081, 2012 https://doi.org/10.1016/j.physb.2011.12.132

[16] M. D. Segall, P. J. D. Lindan, M. J. Probert, C. J. Pickard, P. J. Hasnip, S. J. Clark, and M. C. Payne, "First-principles simulation: ideas, illustrations and the CASTEP code", *Journal of Physics: Condensed Matter*, vol. 14, no. 11 pp. 27-17, 2002 DOI 10.1088/0953-8984/14/11/301

[17] M. Akasaka, T. Iida, T. Nemoto, J. Soga, J. Sato, K. Makino, M. Fukano, and Y. Takanashi, "Non-wetting crystal growth of Mg2Si by vertical Bridgman method and thermoelectric characteristics", *Journal of Crystal Growth*, vol. 304, no. 1 pp. 196-201, 2007 https://doi.org/10.1016/j.jcrysgro.2006.10.270.

[18] E. N. Nikitin, V. G. Bazanov, and V. I.Tarasov, *Sov. Phys. Solid State*

[19] A.V. Chernatynskiy, and S. R. Phillpot, "Anharmonic properties in Mg2X (x= C, Si, Ge, Sn, Pb) from first-principles calculations", *Phys. Rev. B*, vol. 92, no. 6, pp. 064303–064309, 2015 https://doi.org/10.1103/PhysRevB.92.064303

[20] T. Caillat, A. Borshchevsky, and J. P. Fleurial, "Properties of single crystalline semiconducting CoSb3", *J. Appl. Phys.*, vol. 80, no. 8, pp. 4442, 1996. https://doi.org/10.1063/1.363405

[21] M. Umemoto, Y. Shirai, and K. Tsuchiya, "Proc. of the 4th Pacific Rim International Conference on Advanced Materials and Processing (PRICM4)", *The Japan Institute of Metals,* pp. 2145, 2001.

[22] J. Tani, H. Kido, "Thermoelectric properties of Bi-doped Mg_2Si semiconductors", *Physica. B*, vol. 364, no. 1-4, pp. 218, 2005. https://doi.org/10.1016/j.physb.2005.04.017

[23] M. Iida, T. Nakamura, K. Fujimoto, Y. Yamaguchi, R. Tamura, T. Iida, and K. Nishio, "Thermoelectric Properties of Mg2Si1-x-yGexSby Prepared by Spark Plasma Sintering", *MRS Advances*, no. 1, pp. 3971–3976, 2016. DOI: https://doi.org/10.1557/adv.2016.332

[24] M. Akasaka, T. Lida, A. Matsumoto, K. Yamanaka, Y. Takanashi, Imai, and N. Hamada, "The Thermoelectric properties of bulk crystalline n- and p-type Mg2Si prepared by the vertical Bridgman method", *Journal of Applied Physics*., vol. 104, no. 1, pp. 13703-13708, 2008, DOI:10.1063/1.2946722

[25] M. Ekrem, "Mechanical Properties of MWCNT Reinforced Polyvinyl Alcohol Nanofiber Mats by Electrospinnig Method", El-Cezeri Journal of Science and Engineering, vol. 4, no. 2, pp. 190–200, 2017, doi: 10.31202/ecjse.305851.

[26] S. Rai, A. K. Prajapati, and P. K Yadawa, "Effect of Pressure on Elastic Constants and Related Properties of Rare-Earth Intermetallic Compound TbNiAl", *Phys Mesomech*., vol. 26, no. 5, pp 495-504, 2023 https://doi.org/10.1134/S1029959923050028.

[27] I. Oral, and M. Ekrem, "Measurement of the elastic properties of epoxy resin/polyvinyl alcohol nanocomposites by ultrasonic wave velocities", *EXPRESS Polymer Letters,* vol. 16, no. 6, pp. 591-606, 2022. DOI: 10.3144/expresspolymlett.2022.44

[28] C. P. Yadav, and D.K. Pandey, "Pressure dependent ultrasonic characterization of nano-structured w-BN", Ultrasonic, vol. 96, pp 181-184, 2019 https://doi.org/10.1016/j.ultras.2019.01.008

[29] D. R. Clarke. "Materials selection guidelines for low thermal conductivity thermal barrier coatings", *Surf. Coat. Technol*., vol. 163, pp. 67-74, 2003 https://doi.org/10.1016/S0257-8972(02)00593-5/

[30] A. K. Prajapati, S. Rai, and P. K. Yadawa, "Theoretical Investigations on Mechanical and Ultrasonic Characteristics of Gallium Nitride Semiconductor under High Pressure", *Emergent mater*, vol. 5, pp 1985-1993, 2022 https://doi.org/10.1007/s42247-022-00419-2

[31] W. Voigt, Lehrbuch der kristallphysik (mitausschluss der kristalloptik), (Leipzig Berlin, B.G. Teubner), 1928.

[32] T. Morelli, and A. G. Slack, "High lattice thermal conductivity solids in high thermal conductivity of materials", *Goela XVIII*, *Springer Publishe*r., vol. 2, pp. 37–68, 2006

[33] P. K. Yadawa, D. Singh, D. K. Pandey, and R. R. Yadav, "Elastic and Acoustic Properties of Heavy Rare-Earth Metals", *The Open Acoustics Journal*, vol. 2, pp. 61-67, 2009 https://doi.org/10.2174/1874837600902010061.

[34] D. Singh, D. K. Pandey, and P. K. Yadawa, "Ultrasonic wave propagation in rare-earth_monochalcogenides", *centr.eur.j. phys*. , vol. 7, pp. 198-205, 2009 https://doi.org/10.2478/s11534-008-0130-1

[35] R. P. Singh, S. Yadav, D. Singh, G. Mishra, "Theoretical investigation of temperature dependent elastic, thermophysical and ultrasonic properties of Sc-Ti-Zr-Hf quaternary alloy", 2012, vol. 4, no. 1, pp. 33-40. ISSN 2581-8198.

[36] L. Bao, Z. Kong, D. Qu. and Y. Duan, "Revealing the elastic properties and anisotropies of Mg2X (X =Si, Ge and Sn) with different structures from a first-principles calculation", *Materials Today Communications*, vol. 24**,** pp. 2352-4928, 2020 https://doi.org/10.1016/j.mtcomm.2020.101337

[37] A. Guechi, A. Merabet, M. Chegaar, A. Bouhemadou, and N. Guechi, "Pressure effect on the structural, elastic, electronic and optical properties of the Zintl phase KAsSn, first principles study", *J. Alloys Compd.,* vol. 623, pp. 219-228, 2015. https://doi.org/10.1016/j.jallcom.2014.10.114.

[38] S. I. Ranganathan, and M. Ostoja-Starzewski, "Universal Elastic Anisotropy Index." *Phys. Rev. Lett*., vol. 101**,** pp. 9007-9008, 2008.https://doi.org/10.1103/PhysRevLett.101.055504.

[39] S. P. Singh, G. Singh, A. K. Verma, P. K. Yadawa, and R. R. Yadav, "Ultrasonic wave propagation in thermoelectric ZrX2 (X= S, Se) compounds", *Pramana-J. Phys*, vol. 93, pp. 83, 2019. https://doi.org/10.1007/s12043-019-1846-8.

[40] A. K. Jaiswal, P. K. Yadawa, and R. R. Yadav, "Ultrasonic wave propagation in ternary intermetallic CeCuGe compound", *Ultrasonics.,* vol. 89, pp 22-25, 2018. https://doi.org/10.1016/j.ultras.2018.04.009